International Journal of Minerals, Metallurgy and Materials
Volume 27, Number 2, February 2020, Page 264
https://doi.org/10.1007/s12613-019-1847-0

Electrochemical behavior and corrosion resistance of IrO_2–ZrO_2 binary oxide coatings for promoting oxygen evolution in sulfuric acid solution

Bao Liu[1)], *Shuo Wang*[1)], *Cheng-yan Wang*[1,2)], *Bao-zhong Ma*[1,2)], *and Yong-qiang Chen*[1,2)]

1) School of Metallurgical and Ecological Engineering, University of Science and Technology Beijing, Beijing 100083, China

2) Beijing Key Laboratory of Rare and Precious Metals Green Recycling and Extraction, University of Science and Technology Beijing, Beijing 100083, China

(Received: 7 March 2019; revised: 14 April 2019; accepted: 19 April 2019)

Abstract: In this study, we prepared Ti/IrO_2–ZrO_2 electrodes with different ZrO_2 contents using zirconium-n-butoxide ($C_{16}H_{36}O_4Zr$) and chloroiridic acid (H_2IrCl_6) via a sol–gel route. To explore the effect of ZrO_2 content on the surface properties and electrochemical behavior of electrodes, we performed physical characterizations and electrochemical measurements. The obtained results revealed that the binary oxide coating was composed of rutile IrO_2, amorphous ZrO_2, and an IrO_2–ZrO_2 solid solution. The IrO_2–ZrO_2 binary oxide coatings exhibited cracked structures with flat regions. A slight incorporation of ZrO_2 promoted the crystallization of the active component IrO_2. However, the crystallization of IrO_2 was hindered when the added ZrO_2 content was greater than 30at%. The appropriate incorporation of ZrO_2 enhanced the electrocatalytic performance of the pure IrO_2 coating. The Ti/70at%IrO_2–30at%ZrO_2 electrode, with its large active surface area, improved electrocatalytic activity, long service lifetime, and especially, lower cost, is the most effective for promoting oxygen evolution in sulfuric acid solution.

Keywords: electrode; IrO_2–ZrO_2; oxygen evolution reaction; electrochemical behavior; corrosion resistance

1. Introduction

Titanium plates coated with metal oxides have been used as anodes in various electrochemical processes, e.g., water splitting, metal electrowinning, and chlorine production [1–8]. However, the efficiency of the anode is limited by the sluggish kinetics of the oxygen evolution reaction (OER). RuO_2 and IrO_2, which exhibit high conductivity and activity, are considered to be the best catalysts for OER [9–10]. However, the application of RuO_2 as a catalyst for OER is limited by its low corrosion resistance in sulfuric acid solution [11–12]. IrO_2 is more stable than RuO_2 in sulfuric acid solution, but its utilization is limited by its low elemental availability and high cost [13]. Accordingly, finding an efficient, long-term stable and low-cost anode for OER has attracted much attention.

To enhance electrocatalytic performance and reduce cost, active noble metal oxides like IrO_2 and RuO_2 are mixed with other non-active stabilizers to generate mixed-metal-oxide anodes. Various types of these mixed-metal-oxide anodes for OER have been developed, e.g., RuO_2–TiO_2, IrO_2–Ta_2O_5, IrO_2–SiO_2, RuO_2–SnO_2, and IrO_2–SnO_2 [14–19]. Zhang *et al.* [16] reported that the electrochemical properties of IrO_2-based electrodes are improved by doping with SiO_2. Thus far, the Ti/70at%IrO_2–30at%Ta_2O_5 electrode has been the best electrocatalyst for OER in sulfuric acid solution due to its high activity and stability [19–20]. It is generally recognized that the use of proper stabilizers, and even the lack of electrocatalytic activity, can enhance the total activity of a mixed system.

Zirconia (ZrO_2) is an inert oxide that has high corrosion resistance and good thermal stability. ZrO_2 can disperse homogeneously when mixed with other components [21] and can be used as a stabilizer for RuO_2- and IrO_2-based coatings due to its high stability in sulfuric acid solution. Burke and Mccarthy [22] reported that the lifetime of Ti/RuO_2 anodes is prolonged by the incorporation of ZrO_2. In addition, doping with ZrO_2 can promote the dispersion of active components, thereby increasing the number of active sites [23]. Shao *et al.* [24] investigated the effect of ZrO_2 on the crystallization of

Corresponding authors: Cheng-yan Wang E-mail: chywang@yeah.net; Bao-zhong Ma E-mail: bzhma@126.com

IrO_2-based coating and found that ZrO_2 has an inhibitory effect on the growth of IrO_2 crystal. As such, ZrO_2 is a good modifier for the preparation of mixed-metal-oxide anodes.

The Ti/IrO_2–ZrO_2 electrode is typically prepared by thermal decomposition using $ZrCl_4$ or $ZrOCl_2$ [24–25]. This method is simple, although some problems have occurred during the electrode preparation process, e.g., the contamination of the oxide lattice by the residue of chloride ions, which leads to rapid loss of electrode activity [26]. In our previous study, we investigated the effect of calcination temperature on the electrocatalytic performance of the Ti/IrO_2–ZrO_2 electrode prepared using a sol–gel method [27]. The effect of the ZrO_2 content on the surface properties and electrochemical behavior of the Ti/IrO_2–ZrO_2 electrode is not yet fully understood. In this study, we prepared ZrO_2–chemically modified IrO_2 coatings using zirconium-n-butoxide ($C_{16}H_{36}O_4Zr$) and chloroiridic acid (H_2IrCl_6) via a sol–gel route. We performed microstructural analyses and electrochemical measurements to explore the effect of the ZrO_2 content on the surface properties and electrochemical behavior of IrO_2–ZrO_2 binary oxide coatings.

2. Experimental

2.1. Electrode preparation

The Ti/IrO_2–ZrO_2 electrodes were prepared using zirconium-n-butoxide ($C_{16}H_{36}O_4Zr$) and chloroiridic acid (H_2IrCl_6) via a sol–gel route. Details of the electrode preparation procedure were reported in our previous paper [27]. To explore the effect of the ZrO_2 content on the surface properties and electrochemical behavior of Ti/IrO_2–ZrO_2 electrodes, we used Zr contents in the precursor solutions of 10at%, 30at%, 50at%, and 70at%, respectively. We set the calcination temperature to 450°C, and the total oxide loading of the IrO_2–ZrO_2 binary oxide coating was 1.5 mg/cm^2. We prepared the Ti/IrO_2 electrode by the thermal decomposition of chloroiridic acid.

2.2. Characterizations

We performed X-ray diffraction (XRD) measurements to determine the phases of the pure IrO_2 and IrO_2–ZrO_2 binary oxide coatings and identified the XRD patterns using an X-ray diffractometer (Smartlab, Rigaku) with the Cu K_α radiation at 40 kV and 100 mA. We analyzed the surface morphologies using field emission scanning electron microscopy (FESEM, SUPRA55, Zeiss) and determined chemical compositions using energy dispersive spectroscopy (EDS, Thermo-NS7).

We analyzed the electrochemical behaviors of the binary oxide coatings in a three-electrode cell at an electrochemical workstation (CHI660e). We performed the electrochemical measurements in a 0.5-mol/L sulfuric acid solution. The counter electrode was a platinum plate and the reference electrode was a saturated calomel electrode (SCE). To explore the voltammetric behavior and assess the active surface area of the coatings, we performed multiple cyclic voltammetry (CV) measurements ranging from 0 V to 1.2 V at sweep rates ranging from 5 mV/s to 100 mV/s. To assess the electrocatalytic activity, we performed anodic polarization experiments at a sweep rate of 5 mV/s. To correct the IR drop, we performed electrochemical impedance spectroscopy (EIS) analysis. We measured the electrochemical impedance spectra at 1.25 V at frequencies ranging from 10^{-2} Hz to 10^5 Hz. The AC amplitude for the EIS measurement was 5 mV. To determine the service lifetime, we performed accelerated lifetime tests (ALT), for which the applied current density (j) was 2 A/cm^2. We considered the electrode to be deactivated when the cell voltage increased by 5 V.

3. Results and discussion

3.1. XRD analysis

Fig. 1 shows the XRD patterns of the electrodes with different ZrO_2 contents when calcined at 450°C. The peaks observed at 34.64°, 38.48°, 40.24°, 53.00°, and 70.72° are related to the Ti substrate. We found no diffraction peaks related to ZrO_2 in any of the patterns, which implies that at this calcination temperature, the existing ZrO_2 had an amorphous structure. The diffraction peaks corresponding to the (110), (101), and (211) planes are related to the rutile IrO_2. The lattice constant a values of the rutile IrO_2 in the pure IrO_2 coating, the 90at%IrO_2–10at%ZrO_2 coating, and the 70at%IrO_2–

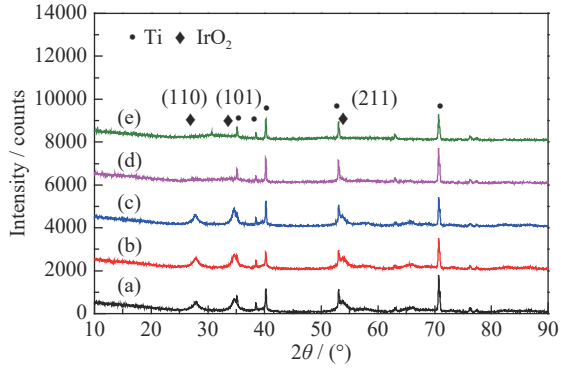

Fig. 1. XRD patterns of the Ti/IrO_2–ZrO_2 electrodes with different molar ratios of IrO_2 to ZrO_2 (Ir : Zr): (a) IrO_2, (b) Ir : Zr = 9 : 1; (c) Ir : Zr = 7 : 3; (d) Ir : Zr = 5 : 5; (e) Ir : Zr = 3 : 7.

30at%ZrO_2 coating were 0.4504 nm, 0.4507 nm and 0.4511 nm, respectively, whereas lattice constant *c* values were 0.3159 nm, 0.3163 nm and 0.3167 nm, respectively. The values of lattice constants *a* and *c* increased with the increase in ZrO_2 content. This indicates that some Zr^{4+} ions are dissolved into the rutile IrO_2 and form a solid solution phase of IrO_2–ZrO_2. Similar results were obtained by Shao *et al*. [24].

Compared to the XRD pattern of the Ti/IrO_2 electrode, the intensities of the rutile IrO_2 diffraction peaks of the Ti/IrO_2–ZrO_2 electrodes with ZrO_2 contents of 10at% and 30at% were higher (Figs. 1(a)–1(c)). This suggests that a slight doping of ZrO_2 promotes the crystallization of the active component IrO_2. When the added ZrO_2 content was higher than 30at%, the diffraction peaks of the rutile IrO_2 disappeared, which suggests that the active component IrO_2 was present as an amorphous structure in the binary oxide coating (Figs. 1(d) and 1(e)). We can conclude that the crystallization of the active component IrO_2 can be controlled by the ZrO_2 content of the coating.

3.2. Surface morphology

Fig. 2 shows FESEM images of the electrodes obtained at low (×3000) and high (×30000) magnifications. In Figs. 2(a) and 2(b), we can observe a compact structure with a small dispersion of needle-like crystals from the Ti/IrO_2 electrode. The lengths of these needle-like crystals range between 80 nm and 100 nm. The results listed in Table 1 suggest that the needle-like crystals are the active component IrO_2.

Compared to the compact IrO_2 coating, all the IrO_2–ZrO_2 coatings exhibited cracked structures combined with flat regions (Figs. 2(c)–2(k)), and the cracks and flat regions had different morphologies. For electrodes with ZrO_2 contents of

Table 1. Elemental composition of the generated needle-like crystal

wt%

Sample	Ti	Ir	Zr	O
IrO_2	1.13	84.46	—	14.41
Ir : Zr = 9 : 1	0.58	75.33	4.74	19.35
Ir : Zr = 7 : 3	1.24	63.01	15.26	20.49

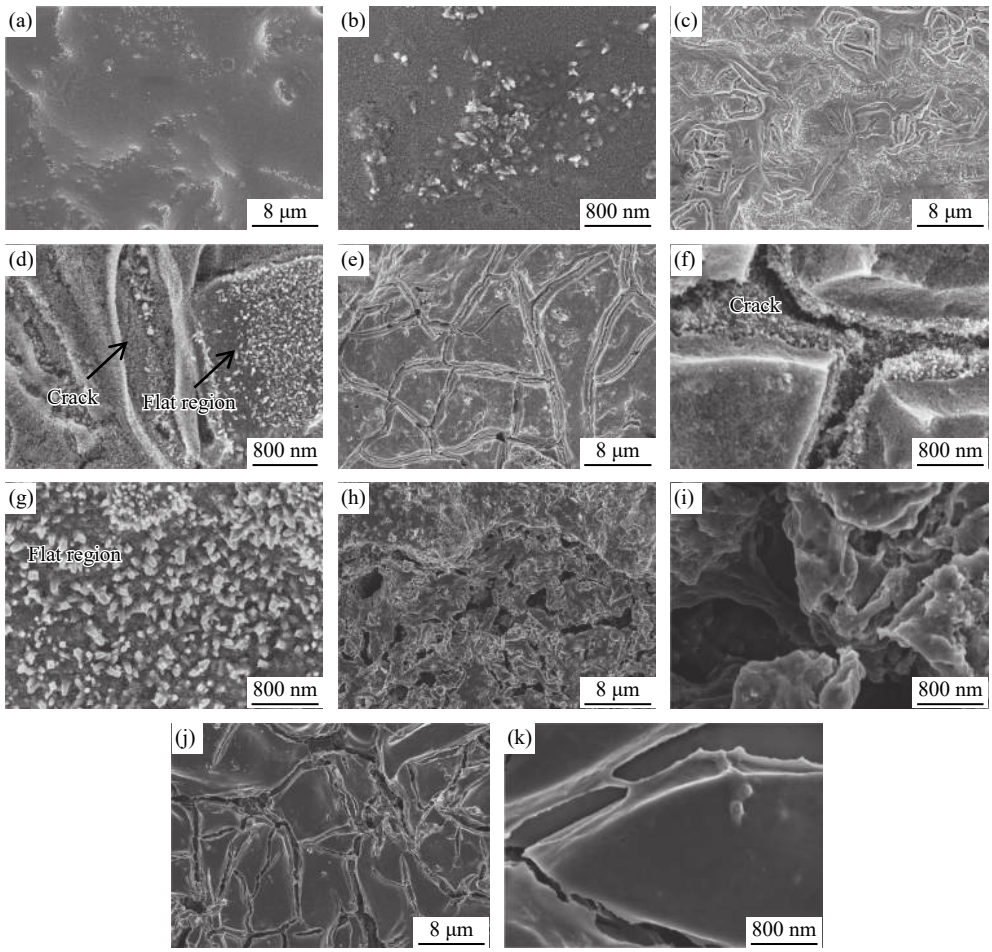

Fig. 2. FESEM images of the Ti/IrO_2–ZrO_2 electrodes with different molar ratios of IrO_2 to ZrO_2 (Ir : Zr): (a, b) IrO_2; (c, d) Ir : Zr = 9 : 1; (e–g) Ir : Zr = 7 : 3; (h–i) Ir : Zr = 5 : 5; (j–k) Ir : Zr = 3 : 7.

10at% and 30at%, dense needle-like nanoscale crystals can form inside cracks and on the flat regions. The length of the needle-like crystals formed inside cracks (40–50 nm) was shorter than those on the flat areas (70–80 nm). The EDS analysis results show that the observed needle-like crystals were enriched with iridium and zirconium, which suggests the generation of an IrO_2–ZrO_2 solid solution phase. When the doped ZrO_2 content increased to 50at% and 70at%, the obtained coatings exhibited an amorphous structure, and we found no needle-like nanoscale crystals either inside the cracks or on the flat regions. This suggests that the crystallization of the active component IrO_2 is inhibited when the added ZrO_2 content is greater than 30at%.

3.3. Electrochemical surface structures

Fig. 3 shows the CV curves of the electrodes with different ZrO_2 contents. We assigned the peaks observed at about 0.6 V vs. SCE to the conversion of Ir(IV)/Ir(III) [28–29]. The peak current of the coatings with ZrO_2 contents of 10at% and 30at% moved to that of the onset potential of OER at about 0.9 V vs. SCE, which is associated with the solid-state redox transaction of Ir(IV)/Ir(V) [16]. Since the active components are the same, the apparent change in the voltammetric response may be correlated with the surface properties [30].

We calculated the voltammetric charge (q^*) by integrating the CV curves. The obtained q^* values can act as a parameter to reflect the active surface area. Considering the active sites for proton exchange, we split the total voltammetric charge (q_{total}) into an "outer" charge (q_{outer}) and an "inner" charge (q_{inner}), whereby the "outer" charge represents active sites that are directly exposed to the electrolyte and the "inner" charge is related to sites that are hidden in cracks and pores. We calculated the values of q_{outer}, q_{inner}, and q_{total} using the following equations [16,31]:

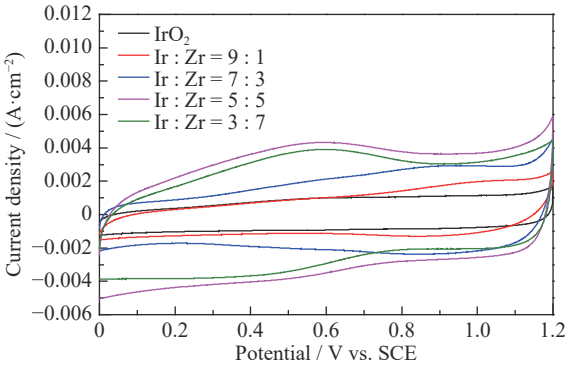

Fig. 3. CV curves of the Ti/IrO_2–ZrO_2 electrodes with different ZrO_2 contents measured in 0.5 mol/L H_2SO_4 solution at a scan rate of 20 mV/s.

$$1/q^* = 1/(q_{inner} + q_{outer}) + C_1 v^{1/2} \quad (1)$$

$$q^* = q_{outer} + C_2 v^{-1/2} \quad (2)$$

$$q_{total} = q_{inner} + q_{outer} \quad (3)$$

where C_1 and C_2 are constants and v is the sweep rate. Based on the above equations, the values of q_{outer} and q_{inner} can be obtained by extrapolating the plots of $1/q^*$ vs. $v^{1/2}$ and q^* vs. $v^{-1/2}$ to $v = 0$ and $v = \infty$.

Fig. 4 shows the calculated q_{total}, q_{outer} and q_{inner} values of the electrodes with different ZrO_2 contents. The q_{total} values of the IrO_2–ZrO_2 coatings were all higher than that of the pure IrO_2 coating, which indicates that doping with ZrO_2 expanded the active surface area of the Ti/IrO_2 anode. The enhanced active surface area of the electrode with ZrO_2 contents of 10at% and 30at% is related to the high crystallinity and small size of the active component. For the coatings with ZrO_2 contents of 50at% and 70at%, the enhanced active surface area is related to the amorphous structure. The q_{total} values of the amorphous coatings were higher than those of the crystalline coating. Xu *et al.* [30] reported that amorphous IrO_2 contributes more to the active surface area than crystallized IrO_2 due to the disorder of the amorphous structure. The q_{outer} value of the crystalline IrO_2–ZrO_2 coatings was higher than the q_{inner} value. For the amorphous IrO_2–ZrO_2 coatings, the q_{inner} value was higher, which suggests that the active surface area of the crystalline IrO_2–ZrO_2 coatings was dominated by the "outer" surface, whereas that of the amorphous IrO_2–ZrO_2 coating was dominated by the "inner" surface.

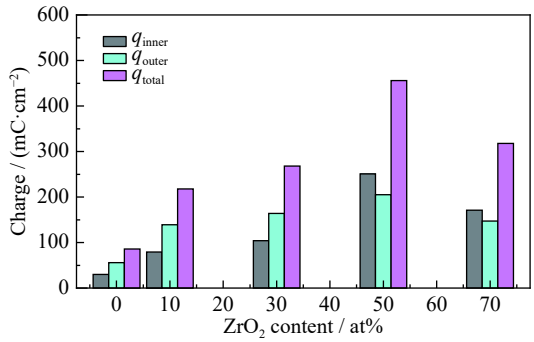

Fig. 4. Voltammetric charges of the coatings calculated by integration of CV curves.

3.4. Electrocatalytic activity and Tafel lines

We determined the apparent electrocatalytic activity of the electrodes by their anodic polarization curves. Fig. 5(a) shows that the apparent electrocatalytic activity of the IrO_2–ZrO_2 coatings increased with increases in the ZrO_2 content, and then decreased when the added ZrO_2 content was

higher than 50at%. The electrode with a ZrO_2 content of 50at% exhibited the most obvious electrocatalytic activity with respect to OER. This was due to the amorphous and porous structure of IrO_2, which contributes more active sites for OER. We observed a reduction in the electrocatalytic activity when the added ZrO_2 content increased to 70at%. Also, ZrO_2 is an oxide with inert properties, so the conductivity and electrochemical performance of the electrode may be reduced by a large incorporation of ZrO_2 into the active oxide coating.

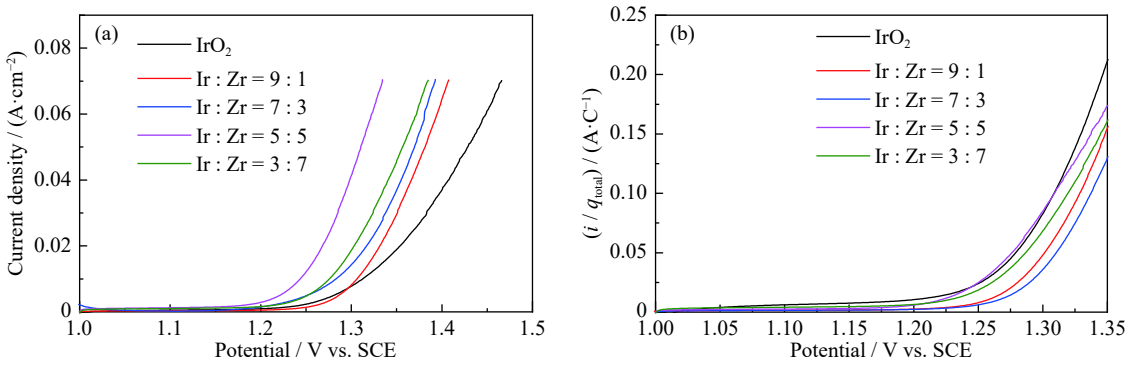

Fig. 5. IR-corrected anodic polarization curves (a) and charge-normalized polarization curves (b) of electrodes with different ZrO_2 contents measured in 0.5 mol/L H_2SO_4 solution at a scan rate of 5 mV/s (i is the current).

We determined the apparent electrocatalytic activity of the electrode based on both the active surface area and its intrinsic catalytic property. To assess the real electrocatalytic effect of ZrO_2 in the coating, we analyzed the charge-normalized polarization curves. Because the q_{total} value represents the total number of active sites on the coating, the electrocatalytic activity at each active site can be estimated by the ratio of the current (i) to q_{total} value [32]. The charge-normalized polarization curves shown in Fig. 5(b) indicate that the normalized electrocatalytic activity of the IrO_2–ZrO_2 coatings was lower than that of the pure IrO_2 coating, which indicates that doping ZrO_2 into the active coating could reduce the intrinsic catalytic properties of each active site. We attribute the enhanced apparent electrocatalytic activity of the zirconia-modified electrodes to the expanded active surface area. The normalized electrocatalytic activities of the coatings with ZrO_2 contents of 50at% and 70at% were higher than those of the coatings with ZrO_2 contents of 10at% and 30at%. We found the enhanced normalized electrocatalytic activity to be correlated with the amorphous structure of the active component IrO_2, which suggests better reactivity of the coating for OER [30]. According to the results of Pfeifer *et al.* [33], the higher reactivity of amorphous IrO_2 is attributable to the electronic defects in the near-surface region of the anionic and cationic framework. We note that the normalized electrocatalytic activity of the amorphous coating with a ZrO_2 content of 70at% was lower than that of the amorphous coating with a ZrO_2 content of 50at%. The reduction of the normalized electrocatalytic activity of the amorphous coating with ZrO_2 content of 70at% can be attributed to the large incorporation of inert ZrO_2.

Next, we fitted IR-corrected Tafel lines to further analyze the electrochemical behavior of the prepared Ti/IrO_2–ZrO_2 electrodes. Fig. 6(a) shows Tafel lines with double-slope behavior. The variation in the Tafel slope indicates an alteration of the electrochemical reaction mechanism.

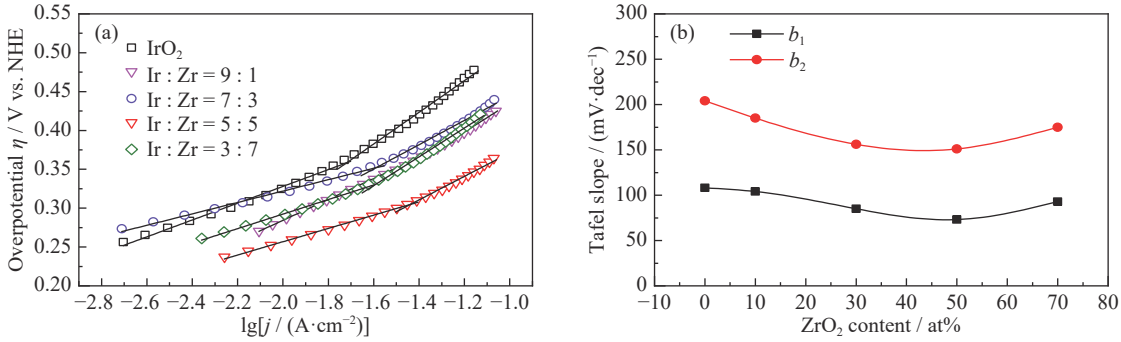

Fig. 6. Tafel lines (a) and Tafel slopes (b) of the electrodes measured in low-overpotential and high-overpotential areas as a function of ZrO_2 content (b_1 denotes the low-overpotential Tafel slope and b_2 is the high-overpotential Tafel slope).

The reaction mechanism for OER is considered to be a three-step process [34–36], for which the first step is the formation of an adsorbed hydroxyl species on the active site (S):

$$S + H_2O \rightarrow S{-}OH_{ads} + H^+ + e^- \quad (4)$$

$$S{-}OH_{ads} \rightarrow S{-}O_{ads} + H^+ + e^- \quad (5)$$

$$2S{-}O_{ads} \rightarrow 2S + O_2 \quad (6)$$

Of these three steps, the rate-determining step (RDS) for OER is considered to be determined by the Tafel slope values. The first, second, and third steps can be considered to be the RDS when the Tafel slope values are about 120 mV/dec, 40 mV/dec, and 15 mV/dec, respectively [37–38].

Fig. 6(b) shows the calculated Tafel slope values of the electrodes with different ZrO_2 contents, where b_1 denotes the low-overpotential Tafel slope and b_2 is the high-overpotential Tafel slope. In the Fig. 6(b), we can see that the Tafel slope values in both the low-overpotential and high-overpotential areas decrease with increases in ZrO_2 content, and then increase when the added ZrO_2 content reaches 70at%. The increased Tafel slope value of the electrode with ZrO_2 content of 70at% can be attributed to the inert properties of ZrO_2, which reduce the electrocatalytic activity. The obtained Tafel slope values of the Ti/IrO_2–ZrO_2 electrodes were all lower than those of the pure IrO_2 electrode, which reveals that OER occurs more easily on IrO_2–ZrO_2 binary oxide coatings than on a pure IrO_2 coating.

In the low-overpotential area, the Tafel slope values ranged between 73 mV/dec and 108 mV/dec, which are not correlated with the abovementioned reaction steps. The OER mechanism is complex as there may be many intermediates in the reaction steps. Considering the existence of the intermediate rearrangement step, the first step can be split as step (4a) and step (4b) [16].

$$S + H_2O \rightarrow S{-}OH^*_{ads} + H^+ + e^- \quad (4a)$$

$$S{-}OH^*_{ads} \rightarrow S{-}OH_{ads} \quad (4b)$$

The S–OH* ads and $S{-}OH_{ads}$ intermediates exhibit the same chemical structure but different energy states. The obtained Tafel slope values of 73–108 mV/dec in the low-overpotential area are consistent with the intermediate rearrangement step (4b). In the high-overpotential area, the Tafel slope values ranged from 151 mV/dec to 204 mV/dec. The first step is considered the RDS for OER.

3.5. EIS measurements

EIS is an effective tool for exploring the surface properties and electrochemical behavior of electrodes, and Fig. 7 shows the resulting Nyquist diagrams and Bode plots. We can observe a small semicircle in the high frequency region of the Nyquist diagram (Fig. 7(a)), which is because the film process occurred in the cracks and pores of the coating. Also, the large semicircle in the low frequency region indicates the charge-transfer process at the electrode/electrolyte interface [39]. In Fig. 7(b), we can see an inductive characteristic at high frequency, which is related to the porous characteristics of the coating [40].

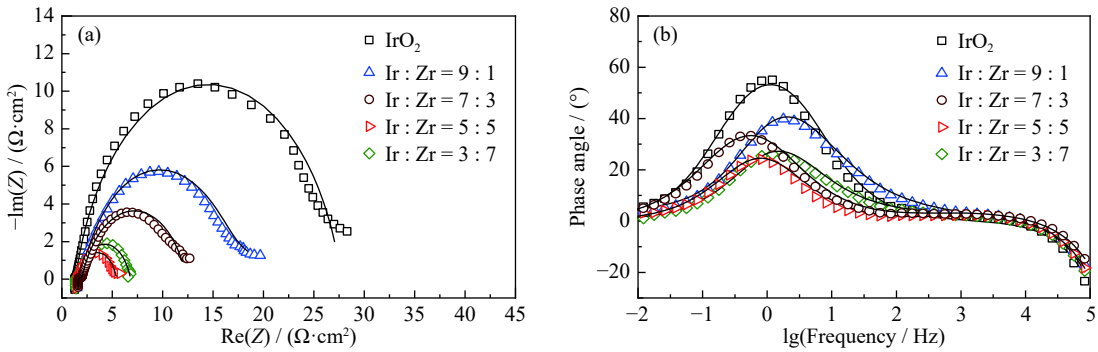

Fig. 7. EIS plots of the electrodes with different ZrO_2 contents: (a) Nyquist diagrams; (b) Bode plots. Z is impedance.

We adopted the equivalent electrical circuit (EEC), $LR_s(R_pC_p)(R_{ct}C_{dl})$, to fit the measured spectra using ZSimpWin software [41], where L denotes the inductance, R_s is the solution resistance, R_p is the film resistance, C_p is the film capacitance, R_{ct} is the charge transfer resistance, C_{dl} is the double-layer capacitance, (R_pC_p) describes the physical response of the porous coating, and the $(R_{ct}C_{dl})$ combination is related to the electrochemical process. Considering the roughness and porous characteristic of the coating, we replaced C_p and C_{dl} with the constant phase elements (Q_p and Q_{dl}), respectively [42]. Based on the obtained Q_p and Q_{dl} values, we can determine the C_p and C_{dl} values [16,43–44].

The results in Fig. 7 show that the measured impedance data are fairly consistent with the simulated results. Table 2 lists the fitted results of the impedance spectra, in which we can see that the R_p values exhibit a rising trend with in-

creases in the ZrO_2 content. The R_p value can be attributed to the film process at high frequency [45]. The increased R_p value indicates an increase in the degree of porosity of the coating [41]. The C_{dl} value, which represents the active surface area, increased from 18.9 mF/cm^2 to 81.6 mF/cm^2 with increases in the ZrO_2 content. We see a decrease in the C_{dl} value to 51.2 mF/cm^2 when the ZrO_2 content increases to 70at%, which is still higher than that of the pure IrO_2 electrode. This reveals that doping with ZrO_2 can increase the number of active sites of the IrO_2-based coating. The R_{ct} values decrease with increases in the ZrO_2 content, and then increase when the added ZrO_2 content reaches 70at%. All the obtained R_{ct} values of the IrO_2–ZrO_2 coatings are lower than those of the pure IrO_2 coating, which indicates that the incorporation of ZrO_2 can improve the electrocatalytic activity of the pure IrO_2 coating.

Table 2. Equivalent circuit parameters of the electrodes, as calculated from the EIS data

Anodes	L / H	R_s / (Ω·cm^2)	C_p / (mF·cm^{-2})	n_p	R_p / (Ω·cm^2)	C_{dl} / (mF·cm^{-2})	n_{dl}	R_{ct} / (Ω·cm^2)
IrO_2	9.972×10^{-7}	1.361	12.1	0.846	0.147	18.9	0.863	26.351
Ir : Zr = 9 : 1	9.063×10^{-7}	1.455	20.6	0.855	0.791	34.2	0.838	20.163
Ir : Zr = 7 : 3	8.620×10^{-7}	1.584	29.3	0.849	1.012	37.5	0.841	9.624
Ir : Zr = 5 : 5	9.453×10^{-7}	1.417	42.7	0.800	1.083	81.6	0.844	3.005
Ir : Zr = 3 : 7	1.026×10^{-6}	1.337	44.2	0.849	1.355	51.2	0.878	4.161

Note: n_p denotes the deviation of Q_p from C_p; n_{dl} stands for the deviation of Q_{dl} from C_{dl}.

3.6. Electrocatalytic stability

Fig. 8 shows the accelerated lifetime of the electrodes with different ZrO_2 contents, in which we can see that the lifetime of the pure IrO_2 electrode is enhanced by the appropriate incorporation of ZrO_2. The electrode with a ZrO_2 content of 30at% obtained the longest lifetime of 306 h. The accelerated lifetimes of the electrodes with ZrO_2 contents of 50at% and 70at% were 70 h and 4 h, respectively. The lifetimes of the Ti/IrO_2–ZrO_2 electrodes significantly decreased when the doped ZrO_2 content was greater than 30at%. Although the electrode with a ZrO_2 content of 50at% exhibited the best electrocatalytic activity for OER, its lifetime was much shorter than that with a ZrO_2 content of 30at%.

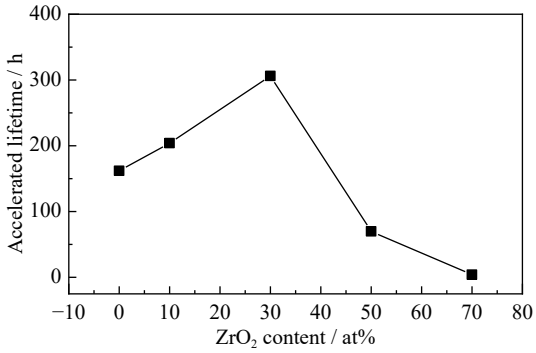

Fig. 8. Accelerated lifetime of the Ti/IrO_2–ZrO_2 electrodes as a function of ZrO_2 content measured in 0.5 mol/L H_2SO_4 solution at a current density of 2 A/cm^2.

The failure of an electrode can be due to several mechanisms, e.g., erosion by gas bubbles, dissolution of the electrocatalyst, or passivation of the Ti substrate [46–47]. Kozo *et al*. [48] reported the deactivation mechanism of a pure IrO_2 electrode, and found that the deactivation of the Ti/IrO_2 electrode can be attributed to the dissolution of the active component IrO_2. Fig. 8 shows that the lifetimes of the electrodes with ZrO_2 contents of 10at% and 30at% were much longer than that of the electrodes with ZrO_2 contents of 50at% and 70at%. This can be attributed to the amorphous structure of the coatings with a high ZrO_2 content. Amorphous IrO_2 shows less electrocatalytic stability than crystallized IrO_2, which can be rapidly dissolved during the OER process [30]. The great dissolution of IrO_2 left a small amount of the effective active component on the coating, thereby leading to the failure of the electrode.

The lifetime (SL) of an electrode is inversely proportional to the applied current density (j). The following equation is often used to calculate the actual SL [49–50]:

$$SL \propto \frac{1}{j^m} \tag{7}$$

where m (1.4–2.0) denotes an empirical parameter obtained from industrial applications. In this study, we adopted an m value of 1.4 to determine the actual SL and obtain the lowest value. The results reveal that the actual SL of the Ti/IrO_2–ZrO_2 electrode with a Zr content of 30at% is about 5 years when the applied current density is 50 mA/cm^2. The actual SL of the Ti/70at%IrO_2–30at%ZrO_2 electrode is about twice as long as that of the Ti/IrO_2 electrode. Comninellis and Vercesi [25] explored the electrocatalytic performance of nine different binary oxide coatings and demonstrated that the Ti/IrO_2–Ta_2O_5 electrode with an IrO_2 content of 70at% exhibits the best electrocatalytic activity for oxygen evolution. Similar results were reported by Mazhari *et al*. [19] and Zhang *et al*. [51]. The fabricated Ti/IrO_2–ZrO_2 electrode with

a ZrO_2 content of 30at% exhibits a comparable electrocatalytic performance with the Ti/70at%IrO_2–30at%Ta_2O_5 electrode. In addition, the metal component Ta_2O_5 is replaced by ZrO_2, which decreases the cost of the electrode preparation. The Ti/70at%IrO_2–30at%ZrO_2 anode, which is characterized by a large active surface area, improved electrocatalytic activity, long service lifetime, and especially, lower cost, is a promising electrode for OER applications.

4. Conclusions

In this study, we prepared Ti/IrO_2–ZrO_2 electrodes with different ZrO_2 contents via a sol–gel route. To explore the surface properties and electrochemical behaviors of the electrodes, we performed physical measurements and electrochemical characterizations. The results of phase and morphology analyses demonstrate that the obtained IrO_2–ZrO_2 binary oxide coating is composed of rutile IrO_2, amorphous ZrO_2, and an IrO_2–ZrO_2 solid solution. The IrO_2–ZrO_2 binary oxide coatings exhibited cracked structures with flat regions. The lengths of the needle-like crystals produced inside the cracks were shorter than those formed on the flat regions. We found a slight incorporation of ZrO_2 to promote the crystallization of the active component IrO_2. However, the crystallization of the rutile IrO_2 was hindered when the added ZrO_2 content was higher than 30at%. The electrocatalytic properties of Ti/IrO_2 can be improved by the appropriate incorporation of ZrO_2. The improved electrocatalytic activity is attributed to the expansion of the active surface area. The anode with a ZrO_2 content of 50at% exhibited the best electrocatalytic activity, although its lifetime was much shorter than the electrode with a ZrO_2 content of 30at%. Considering its electrocatalytic performance, the Ti/70at%IrO_2–30at%ZrO_2 electrode is most suitable for OER application.

Acknowledgements

This work was financially supported by the National Natural Science Foundation of China (Nos. U1802253, 51974025 and 51674026), the Guangxi Innovation-Driven Development Project (No. AA18242042-1), the Beijing Natural Science Foundation of China (No. 2182040), and the Fundamental Research Funds for the Central Universities (FRF22TT-19-001) .

References

[1] D. Devilliers and E. Mahé, Modified titanium electrodes: Application to Ti/TiO_2/PbO_2 dimensionally stable anodes, *Electrochim. Acta*, 55(2010), No. 27, p. 8207.

[2] Y. Zhao, Y.F. E, L.Z. Fan, Y.F. Qiu, and S.H. Yang, A new route for the electrodeposition of platinum–nickel alloy nanoparticles on multi-walled carbon nanotubes, *Electrochim. Acta*, 52(2007), No. 19, p. 5873.

[3] J. L. Lu, S.F. Lu, D.L. Wang, M. Yang, Z.L. Liu, C.W. Xu, and S.P. Jiang, Nano-structured Pd_xPt_{1-x}/Ti anodes prepared by electrodeposition for alcohol electrooxidation, *Electrochim. Acta*, 54(2009), No. 23, p. 5486.

[4] E. Fabbri, A. Habereder, K. Waltar, R. Kötz, and T.J. Schmidt, Developments and perspectives of oxide-based catalysts for the oxygen evolution reaction, *Catal. Sci. Technol.*, 4(2014), No. 11, p. 3800.

[5] S. Siracusano, V. Baglio, A. Di Blasi, N. Briguglio, A. Stassi, R. Ornelas, E. Trifoni, V. Antonucci, and A.S. Aricò, Electrochemical characterization of single cell and short stack PEM electrolyzers based on a nanosized IrO_2 anode electrocatalyst, *Int. J. Hydrogen Energy*, 35(2010), No. 11, p. 5558.

[6] J. Shu, Z.L. Qiu, S.Z. Lv, K.Y. Zhang, and D.P. Tang, Plasmonic enhancement coupling with defect-engineered TiO_{2-x}: A mode for sensitive photoelectrochemical biosensing, *Anal. Chem.*, 90(2018), No. 4, p. 2425.

[7] G.N. Cai, Z.Z. Yu, R.R. Ren, and D.P. Tang, Exciton-plasmon interaction between AuNPs/graphene nanohybrids and CdS quantum dots/TiO_2 for photoelectrochemical aptasensing of prostate-specific antigen, *ACS Sens.*, 3(2018), No. 3, p. 632.

[8] Z.L. Qiu, J. Shu, and D.P. Tang, Near-infrared-to ultraviolet light-mediated photoelectrochemical aptasensing platform for cancer biomarker based on core–shell $NaYF_4$:Yb, Tm@TiO_2 upconversion microrods, *Anal. Chem.*, 90(2018), No. 1, p. 1021.

[9] J. Tang, D.P. Tang, R. Niessner, and D. Knopp, A novel strategy for ultra-sensitive electrochemical immunoassay of biomarkers by coupling multifunctional iridium oxide (IrO_x) nanospheres with catalytic recycling of self-produced reactants, *Anal. Bioanal. Chem.*, 400(2011), No. 7, p. 2041.

[10] X.M. Chen and G.H. Chen, Stable Ti/RuO_2–Sb_2O_5–SnO_2 electrodes for O_2 evolution, *Electrochim. Acta*, 50(2005), No. 20, p. 4155.

[11] F. Moradi and C. Dehghanian, Addition of IrO_2 to RuO_2 + TiO_2 coated anodes and its effect on electrochemical performance of anodes in acid media, *Prog. Nat. Sci*: *Mater. Int.*, 24(2014), No. 2, p. 134.

[12] L.M. Gajić-Krstajić, T.L. Trišović, and N.V. Krstajić, Spectrophotometric study of the anodic corrosion of Ti/RuO_2 electrode in acid sulfate solution, *Corros. Sci.*, 46(2004), No. 1, p. 65.

[13] R. Shan, Z.C. Zhang, M. Kan, T.Y. Zhang, Q. Zan, and Y.X. Zhao, A novel highly active nanostructured IrO_2/Ti anode for water oxidation, *Int. J. Hydrogen Energy*, 40(2015), No. 41, p. 14279.

[14] C.E. Vallet, B.V. Tilak, R.A. Zuhr, and C.P. Chen, Rutherford backscattering spectroscopic study of the failure mech-

anism of (RuO_2 + TiO_2)/Ti thin film electrodes in H_2SO_4 solutions, *J. Electrochem. Soc.*, 144(1997), No. 4, p. 1289.

[15] B.S. Li, A. Lin, and F.X. Gan, Preparation and characterization of Ti/IrO_2–Ta_2O_5 anodes for oxygen evolution used to sulfate electrolysis, *Rare Met. Mater. Eng.*, 36(2007), No. 2, p. 245.

[16] J. J. Zhang, J. M. Hu, J. Q. Zhang, and C.N. Cao, IrO_2–SiO_2 binary oxide films: Geometric or kinetic interpretation of the improved electrocatalytic activity for the oxygen evolution reaction, *Int. J. Hydrogen Energy*, 36(2011), No. 9, p. 5218.

[17] C. Iwakura and K. Sakamoto, Effect of active layer composition on the service life of (SnO_2 and RuO_2)-coated Ti electrodes in sulfuric acid solution, *J. Electrochem. Soc.*, 132(1985), No. 10, p. 2420.

[18] G.C. Pathiraja, N. Nanayakkara, and A. Wijayasinghe, Oxygen evolution reaction of Ti/IrO_2–SnO_2 electrodes: a study by cyclic voltammetry, *Bull. Mater. Sci.*, 39(2016), No. 3, p. 803.

[19] H.A. Mazhari, K. Jafarzadeh, and S.M. Mirali, An investigation of the effect of RuO_2 on the deactivation and corrosion mechanism of a Ti/IrO_2–Ta_2O_5 coating in an OER application, *J. Electroanal. Chem.*, 777(2016), p. 67.

[20] G.P. Vercesi, J. Y. Salamin, and C. Comninellis, Morphological and microstructural the Ti/IrO_2–Ta_2O_5 electrode: effect of the preparation temperature, *Electrochim. Acta*, 36(1991), No. 5-6, p. 991.

[21] R.E. Palma-Goyes, J. Vazquez-Arenas, C. Ostos, R.A. Torres-Palma, and I. González, The effects of ZrO_2 on the electrocatalysis to yield active chlorine species on Sb_2O_5-doped Ti/RuO_2 anodes, *J. Electrochem. Soc*, 163(2016), No. 9, p. H818.

[22] L.D. Burke and M. McCarthy, Oxygen gas evolution at, and deterioration of, RuO_2/ZrO_2-coated titanium anodes at elevated temperature in strong base, *Electrochim. Acta*, 29(1984), No. 2, p. 211.

[23] J. B. Wang, W.P. Zhu, X.W. He, and S.X. Yang, Catalytic wet air oxidation of acetic acid over different ruthenium catalysts, *Catal. Commun.*, 9(2008), No. 13, p. 2163.

[24] Y.Q. Shao, Z.Y. Yi, C. He, J. Q. Zhu, and D. Tang, Effects of annealing temperature on the structure and capacitive performance of nanoscale Ti/IrO_2–ZrO_2 electrodes, *J. Am. Ceram. Soc.*, 98(2015), No. 5, p. 1485.

[25] C.H. Comninellis and G.P. Vercesi, Characterization of DSA®-type oxygen evolving electrodes: choice of a coating, *J. Appl. Electrochem.*, 21(1991), No. 4, p. 335.

[26] A.J. Terezo and E.C. Pereira, Preparation and characterisation of Ti/RuO_2 anodes obtained by sol-gel and conventional routes, *Mater. Lett.*, 53(2002), No. 4-5, p. 339.

[27] B. Liu, C.Y. Wang, Y.Q. Chen, B.Z. Ma, and J. L. Zhang, Effects of calcination temperature on the surface morphology and electrocatalytic properties of Ti/IrO_2–ZrO_2 anodes in an oxygen evolution application, *J. Electrochem. Soc.*, 165(2018), No. 14, p. F1192.

[28] G.R.P. Malpass and A.J. Motheo, Cyclic voltammetric behavior of dimensionally stable anodes in the presence of C1-C3 aldehydes, *J. Braz. Chem. Soc.*, 14(2003), No. 4, p. 645.

[29] W.H. Lee and H. Kim, Oxidized iridium nanodendrites as catalysts for oxygen evolution reactions, *Catal. Commum.*, 12(2011), No. 6, p. 408.

[30] W. Xu, G.M. Haarberg, S. Sunde, F. Seland, A.P. Ratvik, E. Zimmerman, T. Shimamune, J. Gustavsson, and T. Akre, Calcination temperature dependent catalytic activity and stability of IrO_2–Ta_2O_5 anodes for oxygen evolution reaction in aqueous sulfate electrolytes, *J. Electrochem. Soc*, 164(2017), No. 9, p. F895.

[31] L.K. Wu, X.Y. Liu, and J.M. Hu, Electrodeposited SiO_2 film: a promising interlayer of a highly active Ti electrode for the oxygen evolution reaction, *J. Mater. Chem. A*, 4(2016), No. 30, p. 11949.

[32] L.A. Da Silva, V.A. Alves, M.A.P. Da Silva, S. Trasatti, and J.F.C. Boodts, Morphological chemical and electrochemical properties of Ti/(TiO_2–IrO_2) electrodes, *Can. J. Chem.*, 75(1997), No. 11, p. 1483.

[33] V. Pfeifer, T.E. Jones, J.J. Velasco Vélez, C. Massué, M.T. Greiner, R. Arrigo, D. Teschner, F. Girgsdies, M. Scherzer. J. Allan, M. Hashagen, G. Weinberg, S. Piccinin, M. Hävecker, A. Knop-Gericke, and R. Schlögl, The electronic structure of iridium oxide electrodes active in water splitting, *Phys. Chem. Chem. Phys.*, 18(2016), p. 2292.

[34] R.D. Xu, L.P. Huang, J.F. Zhou, P. Zhan, Y.Y. Guan, and Y. Kong, Effects of tungsten carbide on electrochemical properties and microstructural features of Al/Pb–PANI–WC composite inert anodes used in zinc electrowinning, *Hydrometallurgy*, 125-126(2012), p. 8.

[35] T. Audichon, S. Morisset, T.W. Napporn, K.B. Kokoh, C. Comminges, and C. Morals, Effect of adding CeO_2 to RuO_2–IrO_2 mixed nanocatalysts: activity towards the oxygen evolution reaction and stability in acidic media, *ChemElectroChem*, 2(2015), No. 8, p. 1128.

[36] E. Rasten, G. Hagen, and R. Tunold, Electrocatalysts in water electrolysis with solid polymer electrolyte, *Electrochim. Acta*, 48(2003), No. 25-26, p. 3945.

[37] M.H.P. Santana, L.A. De Faria, and J.F.C. Boodts, Effect of preparation procedure of IrO_2–Nb_2O_5 anodes on surface and electrocatalytic properties, *J. Appl. Electrochem.*, 35(2005), No. 9, p. 915.

[38] L.M. Da Silva, L.A. De Faria, and J.F.C. Boodts, Electrochemical ozone production: influence of the supporting electrolyte on kinetics and current efficiency, *Electrochim. Acta*, 48(2003), No. 6, p. 699.

[39] T.A.F. Lassali, J.F.C. Boodts, and L.O.S. Bulhoes, Charging processes and electrocatalytic properties of IrO_2/TiO_2/SnO_2 oxide films investigated by *in situ* AC impedance measurements, *Electrochim. Acta*, 44(1999), No. 24, p. 4203.

[40] J. M. Hu, H.M. Meng, J.Q. Zhang, and C.N. Cao, Degradation mechanism of long service life Ti/IrO_2–Ta_2O_5 oxide anodes in sulphuric acid, *Corros. Sci.*, 44(2002), No. 8, p. 1655.

[41] Y.Y. Hou, J.M. Hu, L. Liu, J.Q. Zhang, and C.N. Cao, Effects of calcination temperature on electrocatalytic activities of Ti/IrO_2 electrodes in methanol aqueous solutions,

Electrochim. Acta, 51(2006), No. 28, p. 6258.

[42] S. Palmas, A.M. Polcaro, F. Ferrara, J.R. Ruiz, F. Delogu, C. Bonatto-Minella, and G. Mulas, Electrochemical performance of mechanically treated SnO_2 powers for OER in acid solution, *J. Appl. Electrochem.*, 38(2008), No. 7, p. 907.

[43] B. Piela and P.K. Wrona, Capacitance of the gold electrode in 0.5 M H_2SO_4 solution: a.c. impedance studies, *J. Appl. Electroanal. Chem.*, 388(1995), No. 1-2, p. 69.

[44] H.T. Yang, H.R. Liu, Z.C. Guo, B.M. Chen, Y.C. Zhang, H. Huang, X.L. Li, R.C. Fu, and R.D. Xu, Electrochemical behavior of rolled Pb–0.8%Ag anodes, *Hydrometallurgy*, 140(2013), p. 144.

[45] V.A. Alves, L.A. da Silva, and J.F.C. Boodts, Surface characterisation of $IrO_2/TiO_2/CeO_2$ oxide electrodes and Faradaic impedance investigation of the oxygen evolution reaction from alkaline solution, *Electrochim. Acta*, 44(1998), No. 8-9, p. 1525.

[46] Z.G. Ye, H.M. Meng, and D.B. Sun, New degradation mechanism of Ti/IrO_2–MnO_2 anode for oxygen evolution in 0.5 M H_2SO_4 solution, *Electrochim. Acta*, 53(2008), No. 18, p. 5639.

[47] G.N. Martelli, R. Ornelas, and G. Faita, Deactivation mechanisms of oxygen evolving anodes at high current densities, *Electrochim. Acta*, 39(1994), No. 11-12, p. 1551.

[48] R. Kötz, H. Neff, and S. Stucki, Anodic iridium oxide films: XPS-studies of oxidation state changes and O_2-evolution, *J. Electrochem. Soc.*, 131(1984), No. 1, p. 72.

[49] Y. Song, G. Wei, and R. Xiong, Structure and properties of PbO_2–CeO_2 anodes on stainless steel, *Electrochim. Acta*, 52(2007), No. 24, p. 7022.

[50] H.T. Yang, B.M. Chen, H.R. Liu, Z.C. Guo, Y.C. Zhang, X.L. Li, and R.D. Xu, Effects of manganese nitrate concentration on the performance of an aluminum substrate β-PbO_2–MnO_2–WC–ZrO_2 composite electrode material, *Int. J. Hydrogen Energy*, 39(2014), No. 7, p. 3087.

[51] W. Zhang, E. Ghali, and G. Houlachi, Review of oxide coated catalytic titanium anodes performance for metal electrowinning, *Hydrometallurgy*, 169(2017), p. 456.